A Nonheme Peroxo-diiron(III) Complex Exhibiting both Nucleophilic and Electrophilic Oxidation of Organic Substrates

Patrik Török,[a] Duenpen Unjaroen,[b] Flóra Viktória Csendes,[a] Michel Giorgi,[c] Wesley R. Browne[*b] and József Kaizer[*a]

Electronic Supplementary Information

Materials

All syntheses were performed under an argon atmosphere unless stated otherwise. Solvents used for the synthesis and reactions were purified by standard methods and stored under argon. The ligand thiabendazole and the metal salts are commercially available used as received from Sigma-Aldrich.

Instrumentation

The crystal evaluation and intensity data collection for the complex **5** was performed on a Bruker-Nonius Kappa CCD single-crystal diffractometer using Mo Kα radiation (λ = 0.71073 Å) at 293 K. Crystallographic data and selected bond lengths and angles are listed in Table S1 and Table S2, and details of the structure determination are given in Figure S1. SHELX–2013[1] was used for structure solution and full matrix least squares refinement on F^2.

UV-vis absorption spectra were recorded on a Cary 60 spectrophotometer (Agilent Technologies, Penang, Malaysia) equipped with a fiber-optic probe with 1 cm pathlength. FTIR spectra were recorded using a Thermo Nicolet Avatar 330 FT-IR instrument (Thermo Nicolet Corporation, Madison, WI, USA). Samples were prepared in the form of KBr pellets. ESI-MS analysis was carried out using a triple quadruple Micromass Quattro spectrometer (Waters, Milford, MA, USA), that was operated in positive electrospray ionization mode. Microanalyses (elemental analysis) were carried out by the Microanalytical Service of the University of Pannonia. Raman spectra were recorded on a PerkinElmer RamanStation at 785 nm, 100 mW at sample.

Synthesis and characterization

[Fe^{II}(L)$_3$](ClO$_4$)$_2$. Thiabendazole (1.500 g, 7.5 mmol) was added under argon to a stirred solution of Fe^{II}(ClO$_4$)$_2$.6H$_2$O (0.901 g, 2.5 mmol) in acetonitrile (20 mL). After stirring for 4 h at room temperature the red solution was filtered and layered carefully with equal amounts of diethyl ether in a Schlenk-tube. After complete diffusion the solvent, it was removed with a cannula together with a minor amount of brown powdery precipitate on the bottom of the Schlenk. The crystalline product was collected, washed with a minimal amount of diethyl ether and dried under vacuum. Yield: 1.428 g (87 %). Anal. Calcd for C$_{30}$H$_{21}$Cl$_2$FeN$_9$O$_8$S$_3$ (858.48): C, 41.97; H, 2.47; N, 14.68. Found: C, 42.02; H, 2.47; N, 14.70. FT-IR spectrum (KBr pellet, cm^{-1}) 3452 m, 3101 m, 1624 w, 1592 w, 1506 w, 1478 w, 1456 w, 1430 m, 1324 m, 1300 w, 1278 w, 1120 s, 1090 s, 1011 m, 994 m, 928 m, 879 w, 837 w, 765 w, 745 m, 625 m. Single crystals were obtained by re-crystallization from acetonitrile with slow diffusion of dichloromethane.

[Fe^{II}(L)$_3$](CF$_3$SO$_3$)$_2$. The above procedure has been applied for the synthesis of this complex. The metal salt was replaced by Fe^{II}(CF$_3$SO$_3$)$_2$. Yield: 1.327 g (81 %). Anal. Calcd for C$_{32}$H$_{21}$F$_6$FeN$_9$O$_6$S$_5$ (957.71): C, 40.13; H, 2.21; N, 13.16. Found: C, 40.08; H, 2.20; N, 13.17. FT-IR spectrum (KBr pellet, cm^{-1}) 3454 m, 3158 m, 3105 s, 2996 w, 1625 w, 1593 w, 1508 w, 1478 w, 1456 w, 1427 m, 1325 m, 1285 vs, 1245 vs, 1226 s, 1163 m, 1030 s, 1012 m, 995 m, 929 w, 881 w, 839 w, 763 w, 746 m, 638 s, 575 w, 518 w.

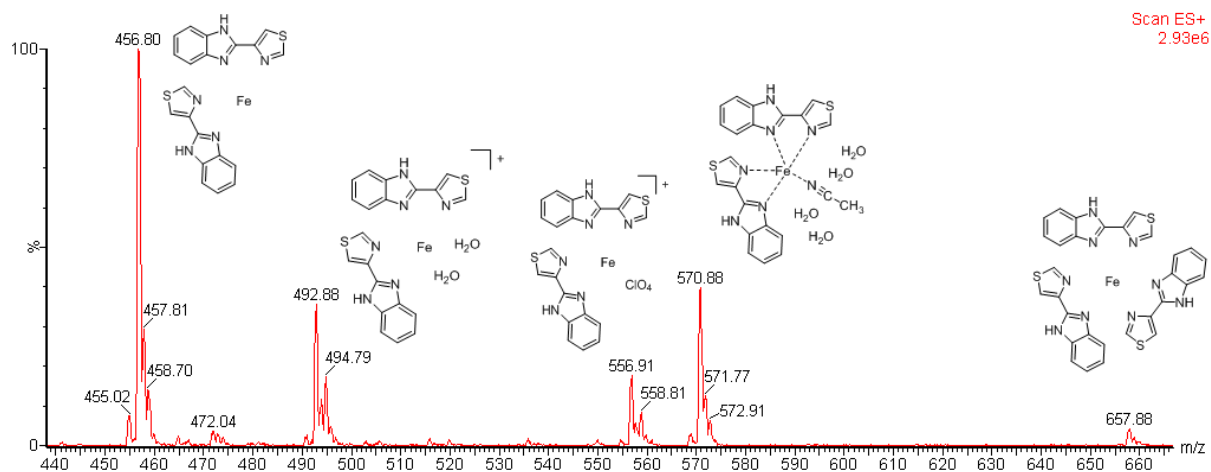1   G. M. Sheldrick, Acta Crystallogr. 2008, **A64** 112

Fig. S1 Electrospray ionization mass spectrum of Fe(L^3)$_3$(ClO$_4$)$_2$. (Calculated m/z of 856.94) The peaks at m/z values 570.88 and 456.80 correspond to the formulae [Fe^{II}(L^3)$_2$(MeCN)(H$_2$O)$_4$] and [Fe^{II}(L^3)$_2$], respectively. The peaks at m/z values 556.91 and 492.88 correspond to the formulae [Fe^{II}(L^3)$_2$(ClO$_4$)]$^+$ (z = 1) and [Fe^{II}(L^3)$_2$)]$^+$ (z = 1), respectively. The peak at m/z value 657.88 corresponds to [Fe^{II}(L^3)$_3$)].
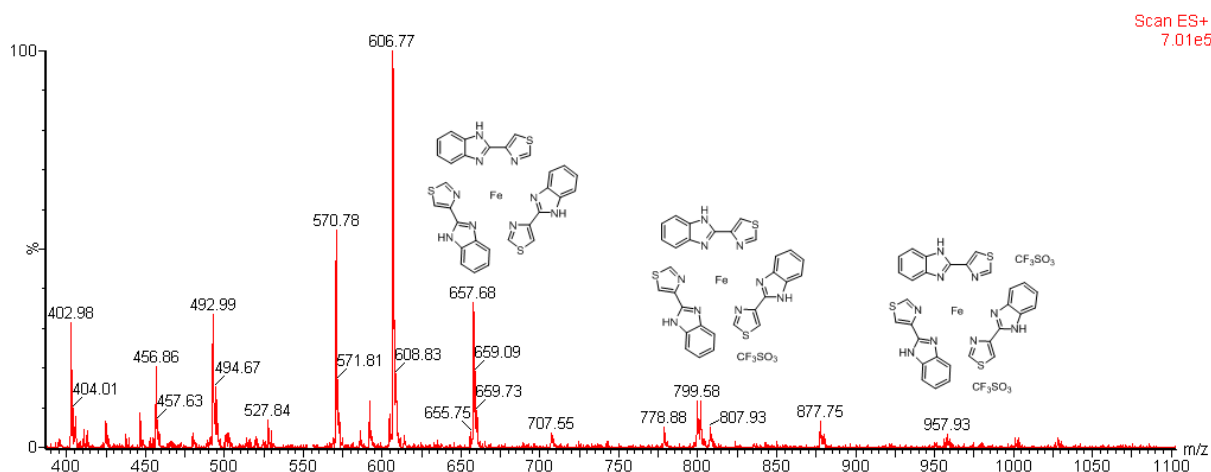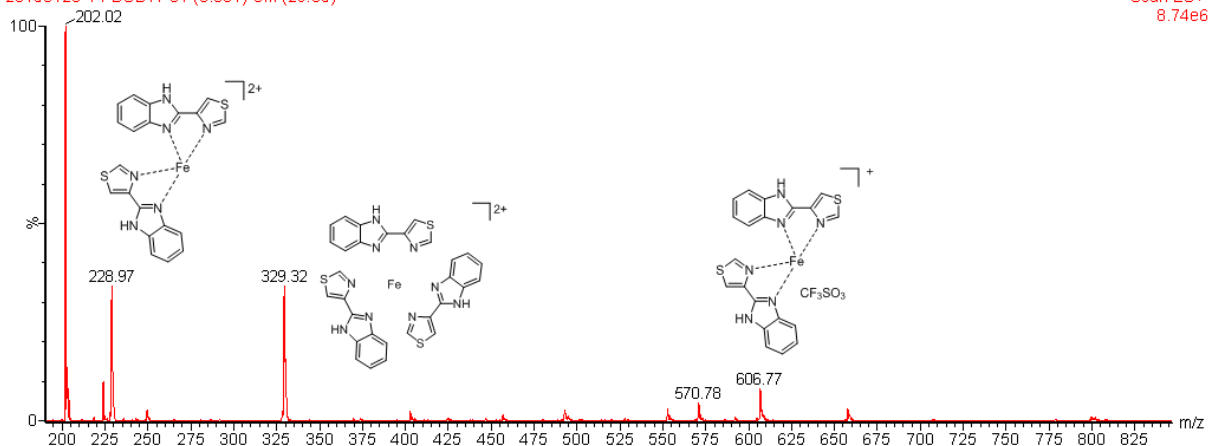

Fig. S2 Electrospray ionization mass spectrum of Fe(L^3)$_3$(CF$_3$SO$_3$)$_2$ (Top and bottom). (Calculated m/z of 956.95). (bottom) The peaks at m/z values 606.77 and 228.97 correspond to the formulae [Fe^{II}(L^3)$_2$(CF$_3$SO$_3$)]$^+$ (z = 1) and [Fe^{II}(L^3)$_2$]$^{2+}$ (Z = 2), respectively. These fragments show similarity to the perchlorate species of the complex (Figure S2). The peak at m/z value 329.32 is the [Fe^{II}(L^3)$_3$)]$^{2+}$ (z = 2). (top) The peaks at m/z values 957.93 and 807.93 and 657.68 correspond to the formulae [Fe^{II}(L^3)$_3$(CF$_3$SO$_3$)$_2$] and [Fe^{II}(L^3)$_3$(CF$_3$SO$_3$)] and [Fe^{II}(L^3)$_3$], respectively.
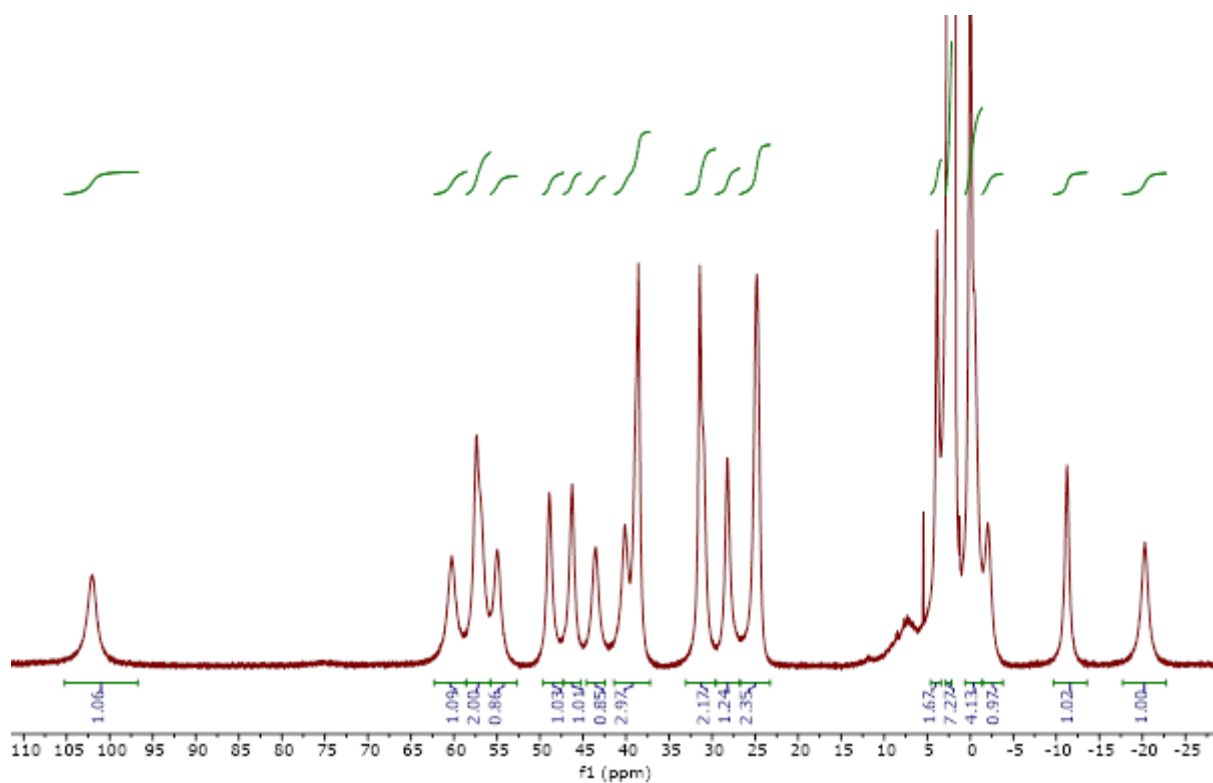
S3

Fig S3 ^{1}H-NMR (400 MHz) of complex **5** in acetonitrile-d_3 at 298 K.
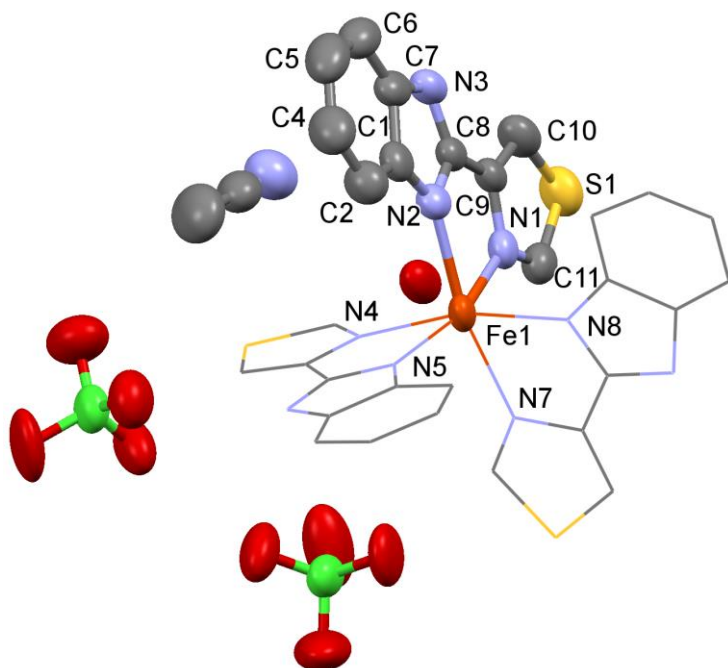

Fig. S4 X-ray structure of **5**. Thermal ellipsoids are plotted at 50% probability level.

Table S1. Summary of crystal data, intensity collection and structure refinement parameters for **1**.

Compound	**1**
Chemical formula	$C_{32}H_{26}Cl_2FeN_{10}O_9S_3$
Formula weight	917.56
Crystal system	triclinic
Space group	P-1
a (Å)	11.6635(11)
b (Å)	12.2558(12)
c (Å)	14.2597(15)
α (°)	86.615(8)
β (°)	80.055(9)
γ (°)	74.102(8)
Volume (Å^3)	1930.79(3)
Z	2
Calc. density (g cm^{-1})	1.578
Temperature (K)	293(2)
Abs. coeff. (mm^{-1})	6.500
F (0 0 0)	936
Obs. reflections	6348
Goodness-of-fit	1.055
R_1[a]	0.1404
wR_2	0.2325

[a] $w=1/[\sigma^2(F_o^2)+(\alpha P)^2+bP]$ and $P = (\max F_o^2,0)+2F_c^2)/3$ $R_1 = \Sigma(|F_o|-|F_c|)/\Sigma(|F_o|)$ and $wR_2 = \{\Sigma[w(Fo^2-Fc^2)^2]/\Sigma[w(F_o^2)^2]\}^{1/2}$.

Table S2. Selected bond distances (Å) and angles (°) for **5**

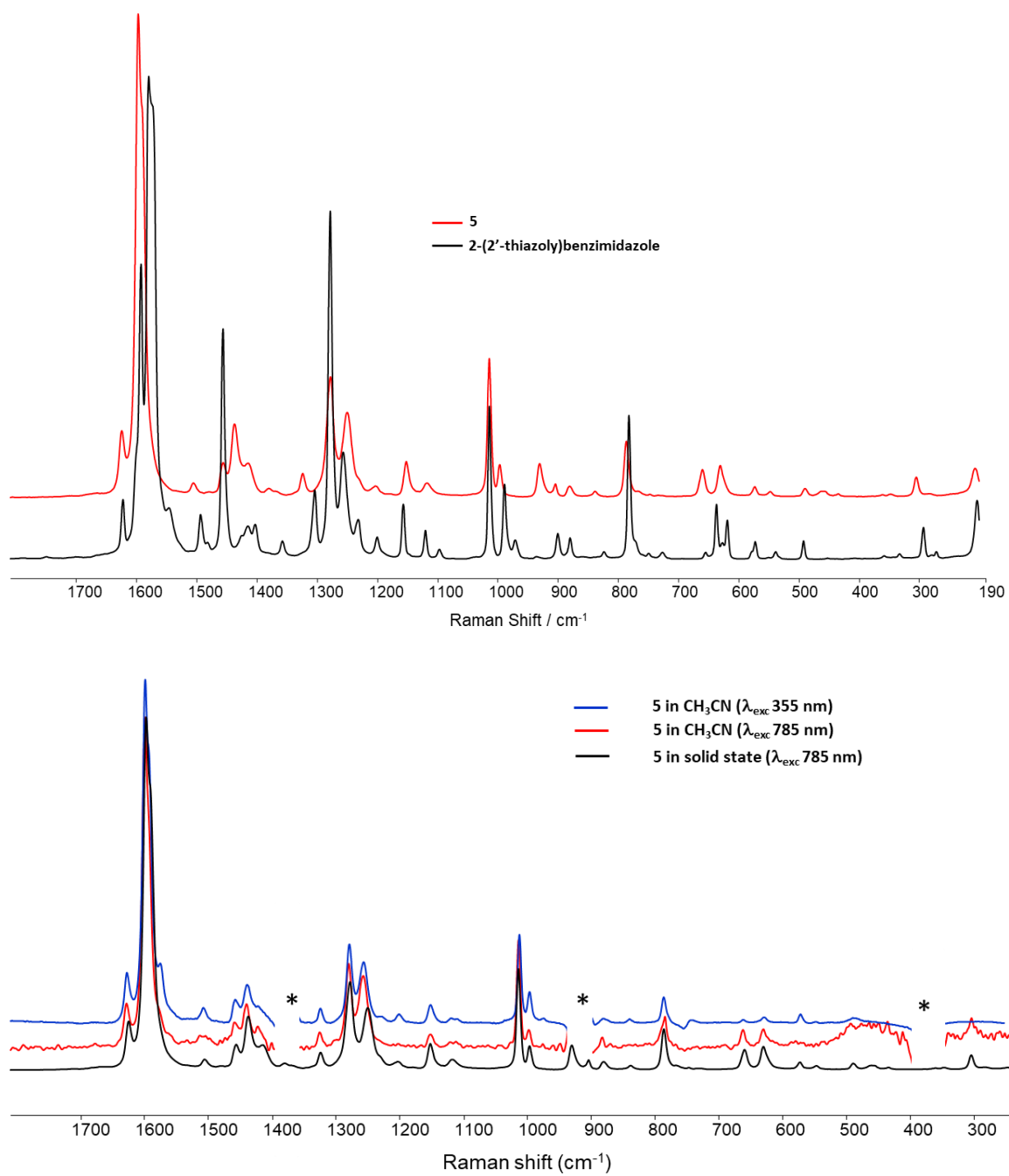| distances		angles	
Fe(1) – N(1)	2.204(7)	N(1)-Fe(1)-N(2)	76.1(3)
Fe(1) – N(2)	2.190(6)	N(4)-Fe(1)-N(5)	76.4(3)
Fe(1) – N(4)	2.251(8)	N(7)-Fe(1)-N(8)	74.5(3)
Fe(1) – N(5)	2.139(8)	N(2)-Fe(1)-N(4)	95.7(3)
Fe(1) – N(7)	2.310(7)	N(2)-Fe(1)-N(7)	166.6(3)
Fe(1) – N(8)	2.165(8)	N(5)-Fe(1)-N(7)	96.4(3)

Fig. S5 (upper) Raman spectra of **5** (red line) and 2-(2'-thiazoly)benzimidazole (black line) in the solid state at λ_{exc} 785 nm, and (lower) Raman specta of **5** in the solid state (black line), in acetonitrile (10 mM) (red line) at λ_{exc} 785 nm and in acetonitrile (0.5 mM) (blue line) at λ_{exc} 355 nm *imperfect solvent substraction

Stoichiometric oxidation:

All reactions were carried out under thermostated conditions at different temperature in 1 cm quartz cuvettes with stirring. The (μ-1,2-peroxo)diiron(III) intermediate was generated in situ with stoichiometric amount of hydrogen peroxide. The appropriate substrate was added to the solution and the oxidation reaction was followed by UV-Vis spectrophotometer between 400 and 1000 nm.

The rate constant was calculated from the equation below.

$$(-d[\mathbf{Fe_2O_2}]/dt = k_{obs}[\mathbf{Fe_2O_2}] = (k_0 + k_{ox}[S])[\mathbf{Fe_2O_2}])$$

Table S3 Kinetic data for the reaction of H_2O_2 with $[Fe^{II}(L^3)]^{2+}$ (**5**)

Exp. entry	$[H_2O_2]_0$ $(10^{-3}$ M)	$[\mathbf{5}]$ $(10^{-3}$ M)	T (°C)	V_i^a $(10^{-6}$ M s$^{-1})$	k $(M^{-1}$ s$^{-1})$
1	1.5	0.50	20	4.75 ± 0.24	6.33 ± 0.51
2	2	0.50	20	6.81 ± 0.32	6.81 ± 0.34
3	3	0.50	20	9.80 ± 1.10	6.53 ± 0.02
4	4	0.50	20	13.7 ± 0.76	6.85 ± 0.02
5	5	0.50	20	17.0 ± 1.57	6.80 ± 0.21
6	10	0.50	20	29.3 ± 1.84	5.86 ± 0.04
7	10	0.33	20	23.1 ± 1.23	7.00 ± 0.25
8	10	0.75	20	53.3 ± 1.70	7.11 ± 0.63
9	10	1.00	20	55.8 ± 2.50	5.58 ± 0.50
					avg. 6.54 ± 0.28

^{a}defined as $-\{d[\mathbf{5}]/dt\}_0 = 2\{d[\mathbf{6}]/dt\}_0$; the initial rate method was applied to minimize the effect of thermal decay on the calculated k values.

Table S4 Relative stability of (μ-1,2-peroxo)diiron(III) intermediates (**3**, **4**, and **6**.

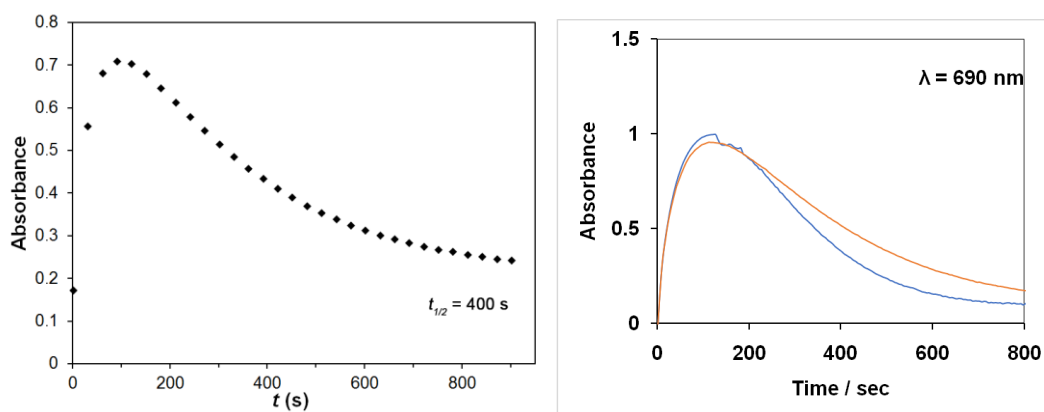| Peroxo intermediate	$t_{1/2}$ s	T K	oxidant	k_{ox} M^{-1} s^{-1}
$[Fe_2(\mu\text{-}O_2)(L^2)_4(CH_3CN)_2]^{4+}$	4740	288	H_2O_2	0.09
$[Fe_2(\mu\text{-}O_2)(L^1)_4(CH_3CN)_2]^{4+}$	1200	288	H_2O_2	0.4
$[Fe_2(\mu\text{-}O_2)(L^3)_4(CH_3CN)_2]^{4+}$	400	288	H_2O_2	1.6

Fig. S6 Left: Absorbance at 705 nm showing loss of the (µ-1.2-peroxo)diiron(III) intermediate generated from **5** with H_2O_2. ($t_{1/2}$ = 400 s), at 288 K in MeCN. Right: Absorbance at 690 nm over time following addition of H_2O_2 (4 equiv) to **5** (2 mM) with ligand (4 mM) at 288 K in CH_3CN. k_{obs} is 0.00286 s^{-1} without additional ligand and 0.0035 s^{-1} with additional ligand present.
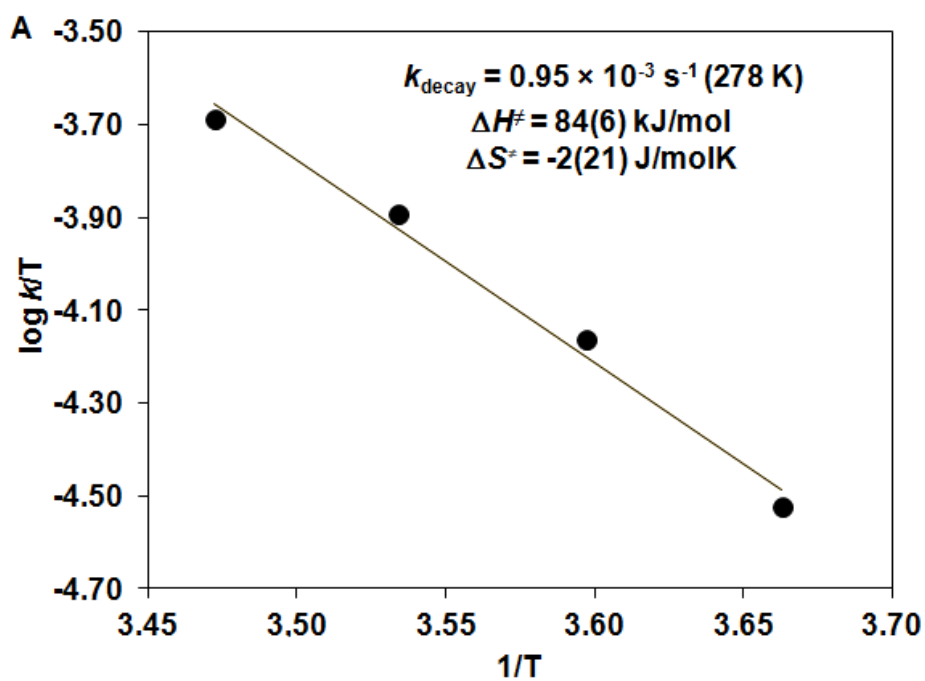

Fig. S7 Eyring plot for the self-decay of $[Fe^{III}_2(\mu\text{-}O_2)(L_3)_2(CH_3CN)_2]^{4+}$ (**6**).

Table S5. Kinetic data for the reaction of **1** with H_2O_2 in MeCN at several temperatures (self-decay data).

N_0	T	$[1]_0$	H_2O_2	k_{obs}	k_2
	(K)	(10^{-3} M)	(10^{-3} M)	(10^{-3} s^{-1})	(M^{-1}s^{-1})
1	273	2	8	0.411	0.0082
2	278	2	8	0.954	0.019
3	283	2	8	1.81	0.036
4	288	2	8	2.96	0.059

Table S6. Kinetic data for the reaction of **1** with benzaldehyde in MeCN at several temperatures.

N_0	T	$[1]_0$	S	k_{obs}	k_{obs}'	k_2	k_2'
	(K)	(10^{-3} M)	(10^{-3} M)	(10^{-3} s^{-1})		(M^{-1}s^{-1})	(M^{-1}s^{-1})
1	288	2	0	0		0.00	
2	288	2	10	29.4	26.44	2.94	2.644
3	288	2	20	58	55.04	2.90	2.752
4	288	2	30	87	84.04	2.90	2.801
5	288	2	40	117	114.04	2.93	2.851
6	273	2	40	22.2		2.22	
7	278	2	40	25.2		2.52	0.606
8	293	2	40	136		3.40	
9	298	2	40	167		4.18	
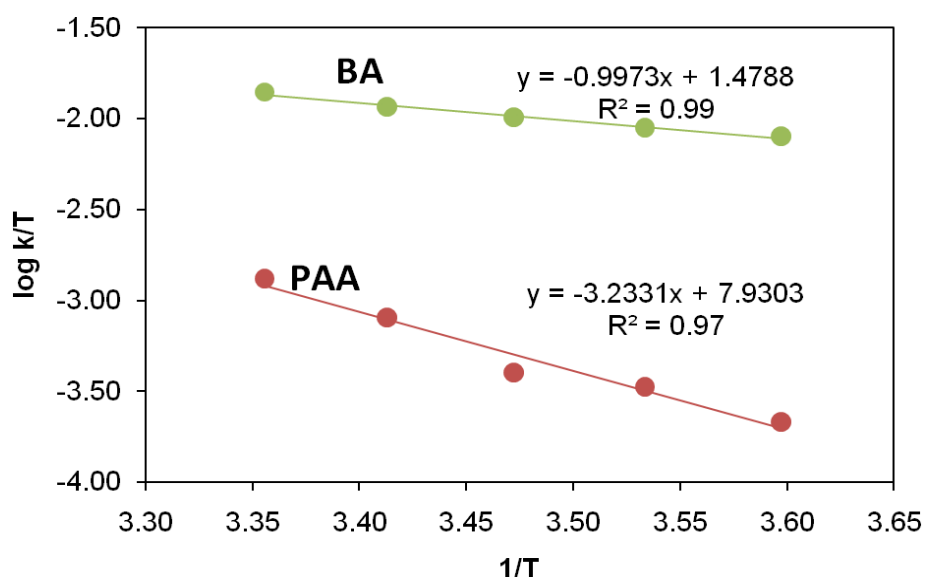
Fig.S8. Eyring plots for the oxidation of BA and PAA with [Fe$^{III}_2$(μ-O$_2$)(L$_3$)$_2$(CH$_3$CN)$_2$]$^{4+}$ (**6**).

Table S7. Kinetic data for the reaction of **1**. with phenylacetaldehyde in MeCN.

(self-decay (T= 5 °C) = 0.954 × 10^{-3} s^{-1})

No	T	[1]$_0$	PAA	k'$_{obs}$	k$_2$
	(K)	(10^{-3} M)	(10^{-3} M)	(10^{-3} s$^{-1)}$	(M^{-1}s^{-1})
1	278	2	0	0	0
2	278	2	25	0.46	0.0184
3	278	2	50	0.93	0.0185
4	278	2	75	1.57	0.0209
5	278	2	100	2.36	0.0236
6	278	2	150	3.12	0.0208
7	278	2	200	4.51	0.0225

Table S8. Kinetic data for the reaction of **1** with 2,6-DTBP in MeCN.

(self-decay (T= 5 °C) = 0.954 × 10^{-3} s^{-1})

N_0	T	$[1]_0$	2,6-DTB-phenol	k'_{obs}	k'_2
	(K)	(10^{-3} M)	(10^{-3} M)	(10^{-3} $s^{-1)}$	($M^{-1}s^{-1}$)
1	278	2	0	0	0
2	278	2	100	0,96	0.0096
3	278	2	200	1,66	0.0083
4	278	2	300	2,25	0.0075
5	278	2	400	3,16	0.0079

Table S9. Kinetic data for the reaction of **1** with 4-methyl-dimethylaniline (4-Me-DMA) in MeCN.

(self-decay (T= 5 °C) = 0.954 × 10^{-3} s^{-1})

N_0	T	$[1]_0$	4-Me-DMA	k'_{obs}	k'_2
	(K)	(10^{-3} M)	(10^{-3} M)	(10^{-3} $s^{-1)}$	($M^{-1}s^{-1}$)
1	278	2	0	0	0
2	278	2	5	0.28	0.055
3	278	2	10	0.83	0.083
4	278	2	15	1.11	0.074
5	278	2	20	1.57	0.079

**Table S10.** Kinetic data for the reaction of **1** with *para*-substituted DMA in MeCN without self-decay

N_0	T (K)	$[1]_0$ (10^{-3} M)	σ_p	4x-DMA (0.1 M)	k_{obs} (10^{-3} s^{-1})	k_{obs}	k_2 ($M^{-1}s^{-1}$)	k_X/k_H	log (k_X/k_H)
1	278	2	0.66	CN	1.02	0.00102	0.0102	0.49	-0.31
2	278	2	0.23	Br	1.54	0.00154	0.0154	0.74	-0.13
3	278	2	0	H	2.07	0.00207	0.0207	1	0
4	278	2	-0.17	CH_3	2.7	0.0027	0.027	1.30	0.12

Table S11. Kinetic data for the reaction of **1** with *para*-substituted benzaldehydes in MeCN

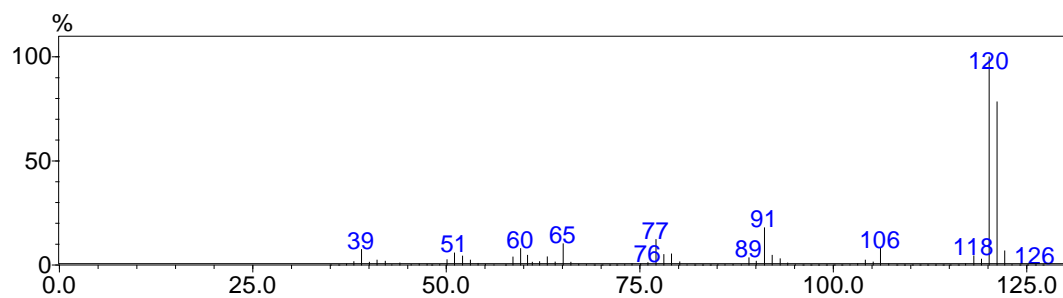| N_0	T	$[1]_0$	σ_p	4_x-PhCHO	k_{obs}	k_2	k_x/k_H	log(k_x/k_H)
	(K)	(10^{-3} M)		(0,04 M)	(10^{-2} s^{-1})	($M^{-1}s^{-1}$)		
1	288	2	-0.27	OCH_3	1.71	0.4275	0.15	-0.84
2	288	2	-0.17	CH_3	3.42	0.855	0.29	-0.53
3	288	2	0	H	11.7	2.925	1.00	0.00
4	288	2	0.23	Cl	24.77	6.1925	2.12	0.33

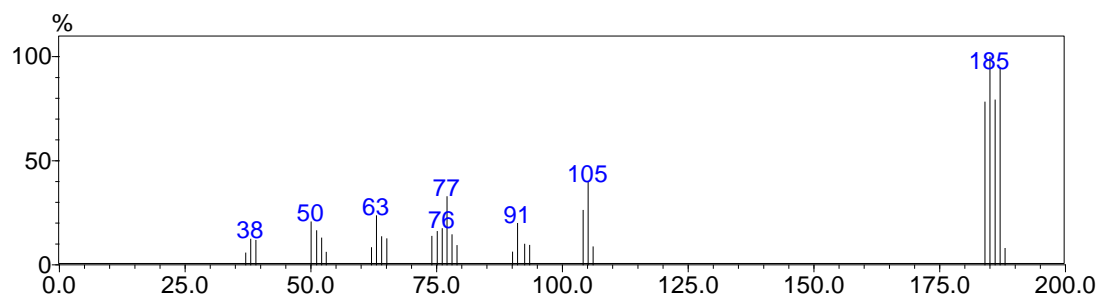**Mass spectral data for oxidation products**

H-DMA→H-MA
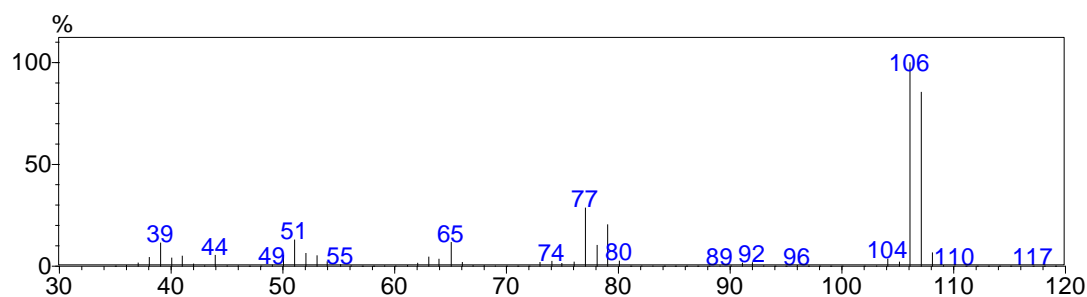
m/z: 107 (85.48 %), 106 (100 %), 77 (28.54 %), 65 (11.73 %), 51 (12.96 %), 39 (11.47 %)
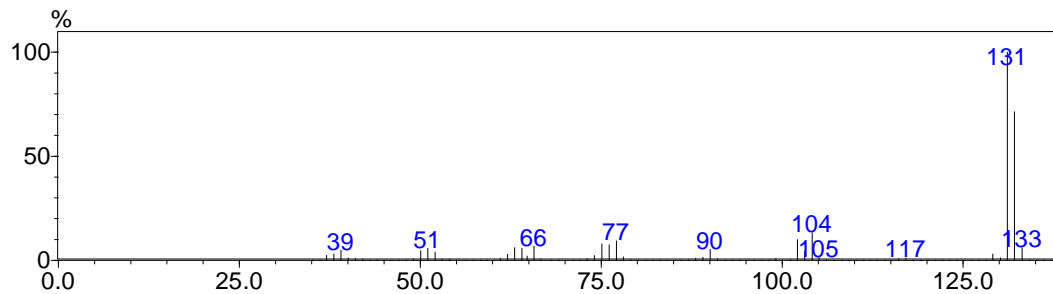
Me-DMA→Me-MA

m/z: 121 (78.6 %), 120 (100 %), 91 (17.96 %), 77 (12.31 %), 65 (10.27 %), 51 (5.82 %), 39 (7.47 %)
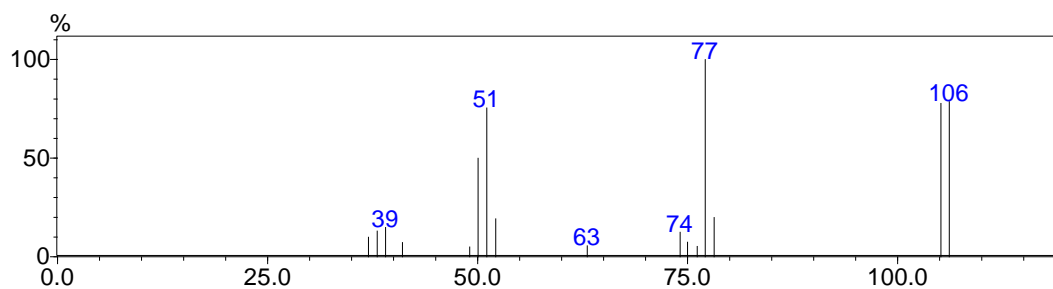
Br-DMA→Br-MA

m/z: 187 (94.71 %), 186 (79.22 %), 185 (100 %), 184 (78.27 %), 105 (39.63 %), 77 (32.82 %), 51 (16.48 %), 39 (11.85 %)
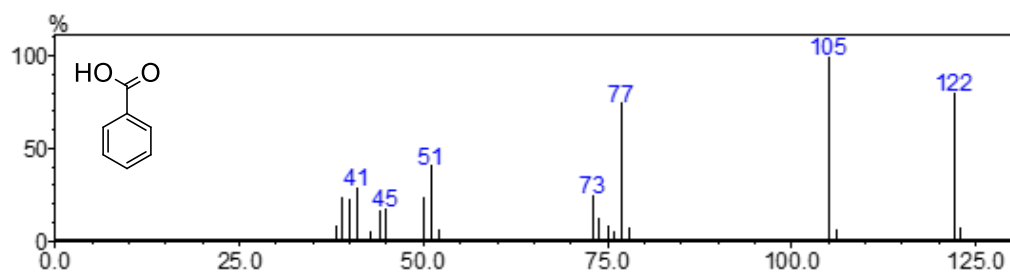
CN-DMA→CN-MA

m/z: 132 (71.44 %), 131 (100 %), 104 (13.22 %), 77 (32.82 %), 51 (5.81 %), 39 (4.91 %)

PAA→BA

m/z: 106 (78.73 %), 105 (77.85 %), 77 (100 %), 51 (75.55 %)

BA→Benzoic acid

m/z: 122 (80.36 %), 105 (100 %), 77 (74.85 %), 51 (40.88 %)